# Impact of flow-induced disturbances during synthesis on the photophysical properties of naphthalene diimide covalent organic frameworks

Veldhuizen, Hugo; van der Zwaag, Sybrand; van der Veen, Monique Ann

**DOI**
10.1016/j.micromeso.2022.112122

**Publication date**
2022

**Document Version**
Final published version

**Published in**
Microporous and Mesoporous Materials

Microporous and Mesoporous Materials 343 (2022) 112122

Contents lists available at ScienceDirect

Microporous and Mesoporous Materials

journal homepage: www.elsevier.com/locate/micromeso

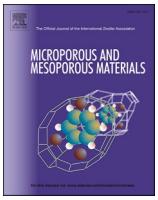

# Impact of flow-induced disturbances during synthesis on the photophysical properties of naphthalene diimide covalent organic frameworks

Hugo Veldhuizen [a], Sybrand van der Zwaag [a], Monique Ann van der Veen [b,*]

[a] Novel Aerospace Materials, Faculty of Aerospace Engineering, Technische Universiteit Delft, 2629 HS, Delft, the Netherlands
[b] Catalysis Engineering, Faculty of Applied Sciences, Technische Universiteit Delft, 2629 HZ, Delft, the Netherlands

ARTICLE INFO

*Keywords:*
Covalent organic frameworks
Stirring synthesis
Taylor-Couette reactor
Naphthalene diimide
Photophysical properties

ABSTRACT

Flow-induced disturbances were applied during the synthesis of a naphthalene diimide covalent organic framework (NDI-COF), which resulted in different COF polymer networks. We discovered that a high intensity of stirring resulted in more aggregated structures on both the micro- and nano-length scale. Subsequently, these structures absorbed light over longer wavelengths due to a relatively higher contribution of intermolecular interactions between the NDI-segments.

## 1. Introduction

Among the material class of hyper-crosslinked polymers with permanent porosity, there is the subclass of covalent organic frameworks (COFs). These polymers are designed to display a degree of crystallinity, which can range from large single crystals to local crystalline domains of few repeating units in an overall amorphous network [1]. The porous structure of a COF depends for a large part on the chemistry and geometry of the building blocks. Moreover, the COF chemistry and polymer network dictate the functional properties, such as redox- and catalytic-activity [2], photovoltaic effect [3] and greenhouse gas capture capacity [4].

Conventional COF synthesis is typically executed in a highly controlled environment (i.e. glass ampules in an oven), in order to carefully regulate the experimental conditions (uniform temperature over long reaction times, inert atmosphere, controlled pressure). In addition, the reaction mixture is usually static, as it is implicitly accepted to be more helpful in the formation of regular, crystalline structures for systems with reversible chemical bonds which would undo topological imperfections. However, the evidence that optimal functional properties are obtained for the best structured networks is weak. In the field of carbon capture, for example, the amorphous counterparts of COFs (i.e. porous organic polymers, POPs) reach similar levels of $CO_2$ capacity [5]. As an additional benefit, POPs have a broader library of linking chemistries to their disposal. Similarly, both COFs and POPs have shown to be promising redox-active materials in electrochemical devices (irrespective of their degree of crystallinity) [6,7]. Theoretically, highly conjugated, crystalline COFs should provide additional electron transport pathways; boosting the device performance [8]. In practice, however, both COFs and POPs often still need to be hybridized with conductive agents for electrode fabrication and their performances remain comparable.

In this work, we deliberately applied flow-induced disturbances during the synthesis of a COF to affect the final polymer network. We distinguished three types of agitation: static, mild, and intense stirring. The COF chosen for this work is structured by naphthalene diimide linkages, since the functional properties of the 1D-polymer variants of these systems have a high dependency on polymer architecture [9,10]. In addition, utilizing poorly-reversible imide-connections in the polymer backbone fits this research well, since the flow-induced disturbances should not affect the in-plane crystallinity as much as more reversible COF systems. The molecular and porous structure of the three NDI-COFs presented here are characterized with FT-IR, PXRD, $N_2$ sorption, and SEM, while the focus of the functional properties is on the photophysical properties.

## 2. Experimental

### 2.1. Materials

All reagents presented in this report were commercially available and used without further purification or treatment. 1,3,5-Tris(4-

* Corresponding author.
*E-mail address:* M.A.vanderVeen@tudelft.nl (M.A. van der Veen).

https://doi.org/10.1016/j.micromeso.2022.112122
Received 7 June 2022; Received in revised form 15 July 2022; Accepted 20 July 2022
Available online 5 August 2022

aminophenyl)benzene (≥93%), 5′-Phenyl-[1,1′:3′,1″-terphenyl]-4-amine (≥98%), and isoquinoline were purchased from TCI Europe N.V (Zwijndrecht, Belgium), 1,4,5,8-naphthalenetetracarboxylic dianhydride (≥95%) and ortho-dichlorobenzene from abcr GmbH (Karlsruhe, Germany) and N-methyl-2-pyrrolidone from Acros Organics B.V.B.A (Geel, Belgium).

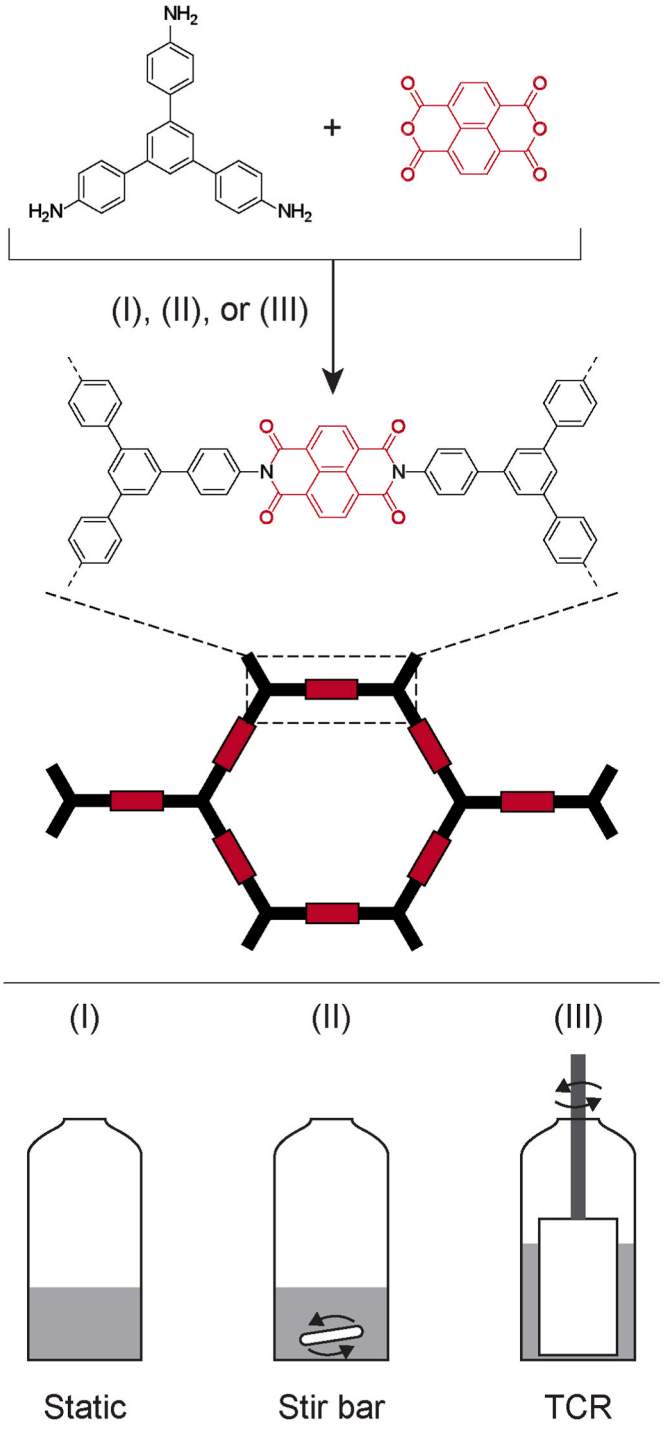


**Fig. 1.** Schematic overview of COF formation by polycondensation of TAPB and NDA, and the three different synthesis methods: (I) static: no agitation, (II) continuous stirring with a stir bar, and (III) high-intensity stirring in a Taylor-Couette reactor (TCR).

### 2.2. Covalent organic framework synthesis

Fig. 1 shows a schematic overview of the COF chemistry and different synthesis methods employed in this research. All syntheses were performed in borosilicate glass flat-bottom 100 mL cylindrical reactors, using the monomers 1,3,5-tris(4-aminophenyl)benzene (TAPB), and 1,4,5,8-naphthalenetetracarboxylic dianhydride (NTCDA). COFs named 'static' were not agitated during synthesis, while 'stir bar' COFs were continuously stirred with a conventional stir bar. Lastly, intense stirring was applied by utilizing a cylindrical mechanical stirrer in the reactor, resembling a Taylor-Couette reactor (TCR) [11]. Considering the rotational speed and dimensions of the reactor and stirrer, the continuous and homogeneous shear rate for the TCR method is estimated at 250 $s^{-1}$. On the other hand, the stir bar method imposes a highly heterogeneous shear rate; ranging from $\dot{\gamma}_{min} = 4.5\ s^{-1}$ to a very local maximum at the stir bar tip of $\dot{\gamma}_{max} = 190\ s^{-1}$ (Fig. S2). The detailed synthesis protocols of static, stir bar and TCR COFs are documented in the Supporting Information, as well as the details on characterization techniques. The data concerning the characterization of the materials described in this work can be accessed and used by others for further studies at 4TU.ResearchData [30].

## 3. Results and discussion

Completion of the polycondensation reactions of the stir bar-, and TCR-COFs was confirmed by FT-IR (Fig. S4). All three different syntheses yielded polyimide polymers, which was apparent from the appearance of symmetric (1674 $cm^{-1}$) and asymmetric C═O (1715 $cm^{-1}$) imide peaks and C–N imide peaks (1339 $cm^{-1}$), combined with the disappearance of characteristic functional group vibrations of the originating monomers. No significant molecular differences between the differently agitated syntheses were observed. The thermal stabilities of the three COFs are similar as well (Fig. S5), with the main decomposition at a maximum around the temperature range of 640–660 °C. In addition, a minor weight loss (5–10 wt %) is present in the region of 300–500 °C for all COFs. The origin of this weight loss is yet unclear: it could be trapped solvent species, unreacted monomer, and/or water release due to cyclization reactions of unreacted poly(amic acid).

PXRD measurements revealed that all COFs display similar crystalline order, being only on a short, local length scale (Fig. S6), as is also the case for previously reported COFs with the same polymer chemistry [6,12]. The static-, stir bar-, and TCR-COFs all show (100) and (200) reflections (where the former at 2.8° corresponds to the expected hexagonal size of 3.1 nm; previously investigated by our group through molecular modelling) [6]. Agitation during synthesis did influence the porosity of the COFs significantly, which we investigated by measuring nitrogen sorption isotherms (Fig. 2A). While the stir bar-COF shows very similar isotherm curves to the static-COF, the TCR-COF's porosity decreased notably: in particular the isotherm knee around 0.25 $P/P_0$ became less pronounced and the increase in $N_2$ uptake between 0.05 and 0.25 $P/P_0$ diminished. These observations indicate a reduction in small mesopore volume and a broader pore size distribution (PSD) of TCR-COFs. The PSDs were calculated based on the adsorption branches of the COFs (Fig. 2B), using a quenched solid density functional (QSDFT) model that is based on carbon materials with slit and cylindrical pore geometries [13]. The fitting curves of the PSD calculations are provided in the Supplementary Fig. S7. Finally, the overall Gurvich pore volume based on the $N_2$ uptake at 0.9 $P/P_0$ are 0.49, 0.50 and 0.37 $cm^3\ g^{-1}$ for the static-, stir bar- and TCR-COFs respectively.

SEM micrographs of the COFs prepared by the three synthesis methods are shown in Fig. 3. First, in the zoomed-out micrographs (Fig. 3 left), the large agglomerates (ranging from 20 to 200 μm) of the static-COFs stand in stark contrast to the more uniform and smaller particles of the stir bar- and TCR-COFs (sizes between 10 and 20 μm). Secondly, on a smaller length scale (Fig. 3 right) a clear distinction in morphology is observed when comparing non-agitated to agitated COFs.

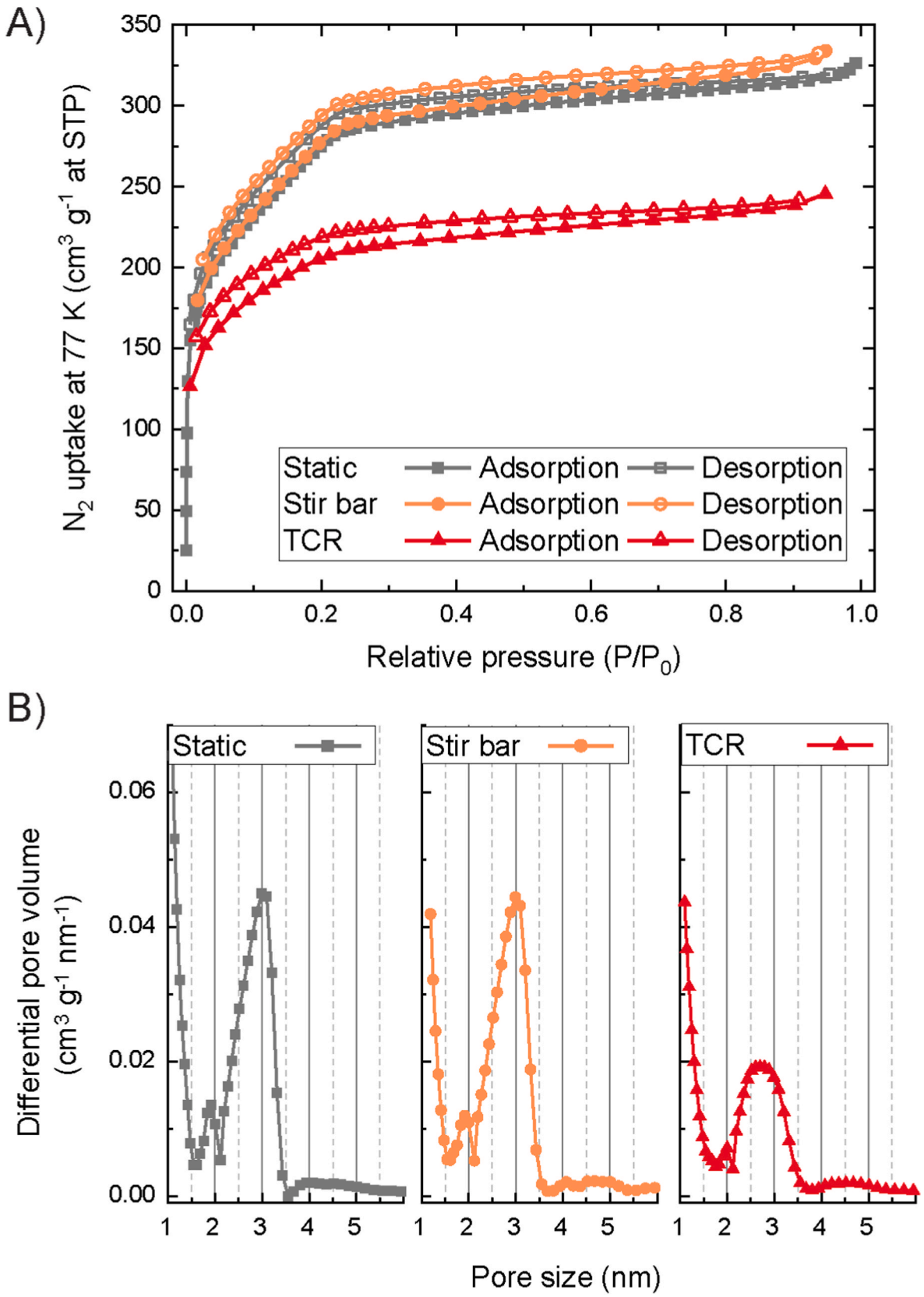


**Fig. 2.** A) Nitrogen gas sorption isotherms of static-, stir bar- and TCR-COFs. B) Pore size distributions of static-, stir bar- and TCR-COFs based on the adsorption branch of the nitrogen isotherms and a QSDFT (slit-cylindrical pore geometry) carbon model.

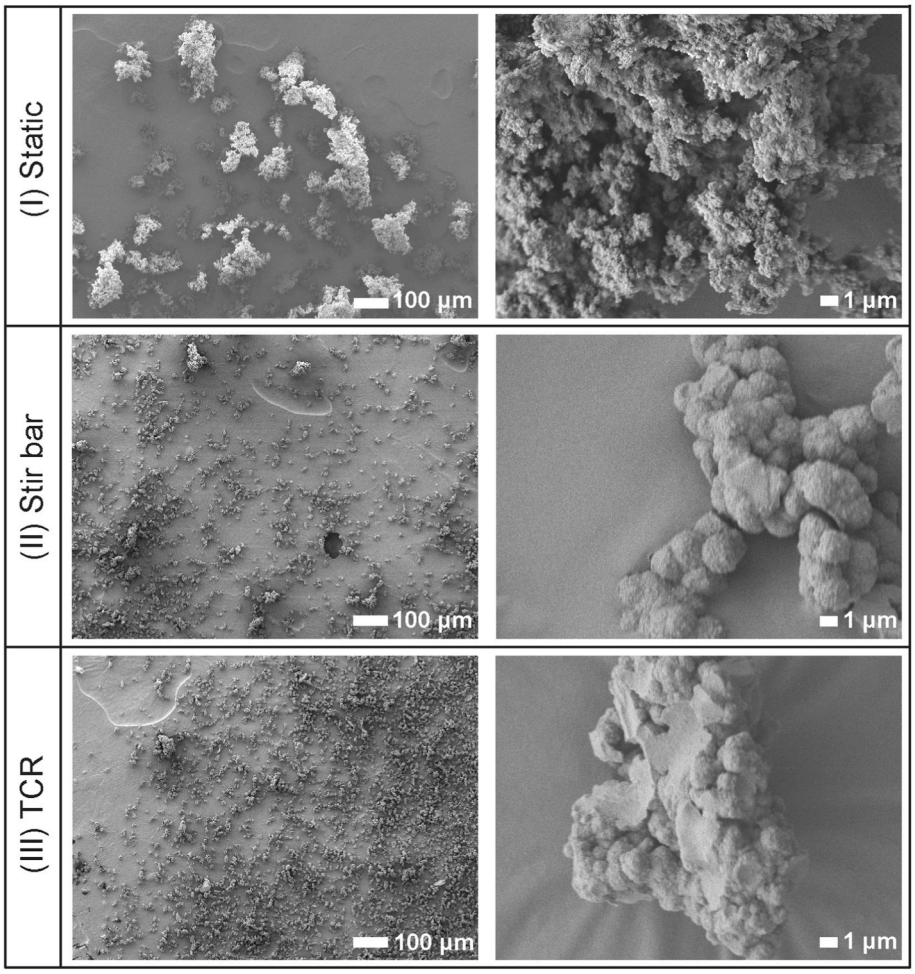


**Fig. 3.** SEM images of static-, stir bar-, and TCR-COFs. The scale bars are the same for each column: left 100 µm, right 1 µm.

The 'open', dendritic-like structures of static-COFs are distinguished from the more collapsed, aggregated-spherical structure of the stir bar- and TCR-COFs.

Evidently, the shear rates applied during the synthesis of NDI-COFs have a significant effect on the final polymer network, without affecting the polymer chemistry or in-plane crystallinity. This observation is quite interesting, since the majority of published COF syntheses (where optimization is directed towards the highest degree of crystallinity) invariably involve only static reaction mixtures under solvothermal conditions and only effects of polymer chemistry, temperature and time on morphology are captured.

Regarding the porous structures of the three polymer powders, the mesopore volume derived from the crystalline pores of 3.1 nm as observed by PXRD, likely originates from local areas of stacked hexagonal units within the polymer. The clear maximum in PSDs of static- and stir bar-COFs suggest a relatively uniform stacking mode within these local areas of stacked hexagonal units. In contrast, the stacking mode is more random with larger offsets for TCR-COFs, since this would yield a reduction in mesopore volume and a broader maximum [14]. In addition, the mesopore volume could also be reduced through pore blocking within the polymer aggregates or interpenetration of neighbouring local stacks. In both cases, this decrease in mesopore volume of TCR-COFs suggests a high degree of aggregation on the nanoscopic scale. Furthermore, SEM images at low magnification show that the static COF has a much larger agglomerate size than the other two powders. This was to be expected, since sufficient stirring intensities break up loosely bound particles while the agglomerates grow [15]. However, when examined at higher magnification the stir bar- and TCR-COFs display larger single particle sizes, while appearing increasingly more aggregated. We expect that the effects of stirring in this regard are two-fold: (1) homogeneously distributed monomers in their stochiometric ratios causing a higher molecular weight and subsequently larger, more uniform particles [16], and (2) additional flow forces acting on the forming particles causing the polymer network to be formed in a more inward facing, collapsed manner [17]. According to these results, we have employed a facile approach towards morphology control in NDI-COF systems.

Structural control on the nanoscale in NDI-based systems may play a large role in controlling their photophysical properties. This phenomenon has been observed in mesoporous silicas containing chemically similar perylene diimide segments [18]. Also in the case of polyimine COFs, Deng and coworkers have recently shown how careful regulation of interlayer packing through COF chemistry can enhance the optical properties [19]. Therefore, we investigated how the observed structural changes in the COFs presented here, affected these properties. We observed stark differences in their UV–Vis spectra (Fig. 4A). Each COF has a different $\lambda_{max}$, being 393 nm for static, 417 nm for stir bar, and 446 nm for TCR COFs, where red-shifts of these maxima typically indicate longer conjugation lengths. Furthermore, the absorbance intensity of the secondary shoulder peak (in the range of 490–510 nm) is much more a distinct peak in the TCR-COFs.

In order to attribute the observed changes in spectral features to their chemical and structural origins, we synthesized a model compound that represents an isolated repeating unit of the COF framework (Fig. 4B). The 0–2, 0–1, and 0-0 absorption bands of this molecule at $\lambda_{max}$ of 345, 361, and 380 nm respectively are clearly visible in the liquid state and

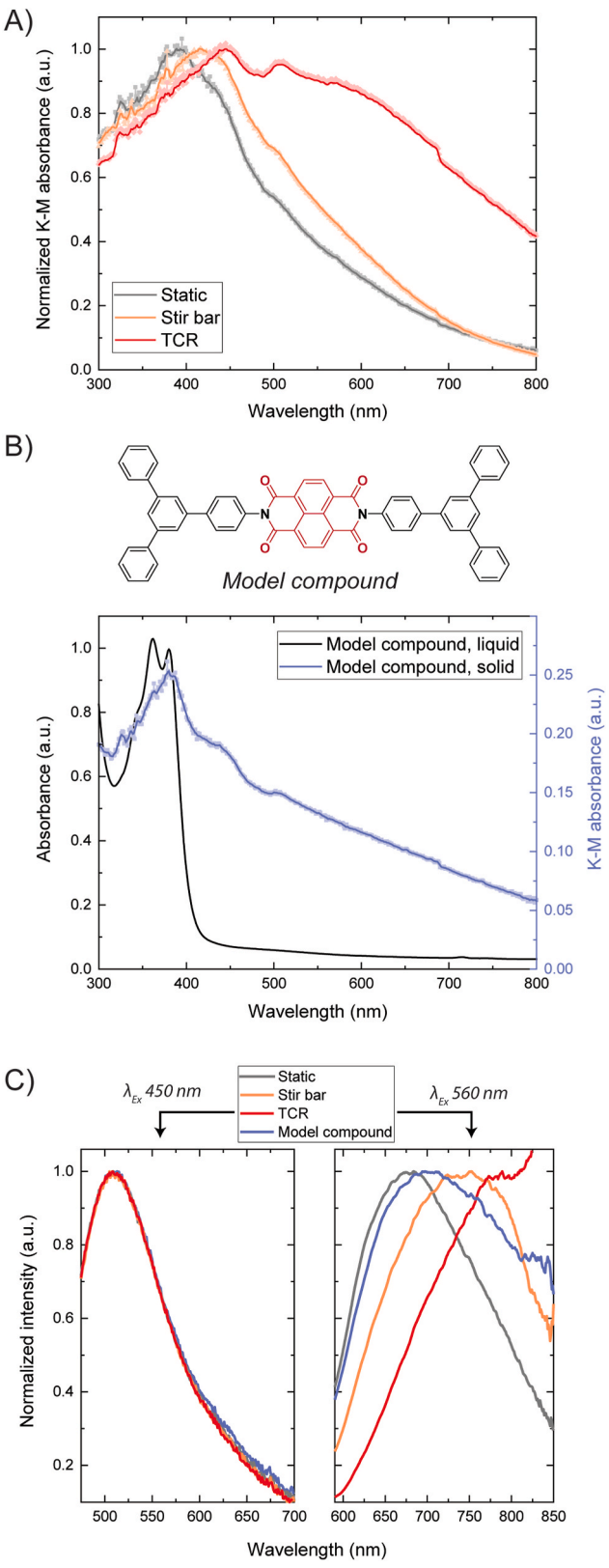


**Fig. 4.** A) Kubelka-Munk absorbance spectra of static-COF, stir bar-COF and TCR-COF measured by diffuse reflectance spectroscopy. B) UV absorbance spectrum of the model compound: dissolved in toluene (black line) and in the solid state (blue line, K-M absorbance). The step-change around 687 nm is an artefact of the measurement. C) Photoluminescence spectra of static-COF, stir bar-COF and TCR-COFs and the model compound, at excitation wavelengths of 450 (left) and 560 (right) nm. (For interpretation of the references to colour in this figure legend, the reader is referred to the Web version of this article.)

are in line with characteristic π-π* transitions of other NDI-based materials [20]. The UV spectrum of the same model compound in the solid state, however, shows light absorption over a broad range of wavelengths with distinct spectral features. Next to the NDI π-π* transition at 380 nm, we observed two shoulder peaks between 430 - 450 nm and 496–510 nm. These differences in UV absorbance behaviour from the solvated state in NDI-based systems has extensively been studied and are often attributed to self-organization [20]. The presence of two distinct shoulders at longer wavelengths suggests multiple different intermolecular stacking modes [21]. In NDI-based small molecule systems, this has been further explored by combining these molecules with electron-rich aromatic donors (e.g. pyrene or derivatives thereof). Here, charge transfer (CT) complexes, that are a result of electrons in the HOMO of the donor promoted to the LUMO of the NDI-unit, are observed through the appearance of a characteristic broad absorption band centred around 500–550 nm [22,23]. It is possible that the phenyl rings of the triphenylbenzene segments acted as electron donors in the self-organization of the model compound [24], as well as in local areas within the polymer networks of the COFs. The position and intensity of this CT band relies on multiple factors, such as the orbital overlap and solvent effects (chemical environment). Lastly, photoluminescence (PL) measurements were conducted to investigate the effect of differently packed polymer networks on excited-state properties. Excitation at 450 nm triggered the same emission behaviour for all COFs and the model compound (Fig. 4C), implying that this is caused by the main absorption bands of NDI segments that are present in all materials. On the other hand, excitation at 560 nm red-shifted the emission spectra of the COFs and model compound in a similar trend to the absorption spectra. This PL behaviour has been observed in NDI-based polymers and is indicative of a large content of inter-polymer NDI aggregates present in TCR-COFs, which would yield red-shifted aggregation-induced emission [9,25].

The distinct nanostructures of the COFs investigated here lead to distinctly different photophysical properties. The differences in absorption spectra between the static- and stir bar COFs are relatively small compared to their differences with the TCR-COF. These trends are similar to the trends observed when comparing the PSDs and mesopore volume. Thus, we were able to correlate the TCR-synthesis method to a different nanostructure (through observation of a lower mesopore volume), and subsequently to the COF's light absorbance and aggregation-induced emission. While engineering the optical properties in COFs typically relies on chemically altering the building blocks [25–27], we have shown that changing the processing-side of the synthesis may lead to similar changes. In a similar vein, we anticipate that mechanochemical concepts such as ball milling synthesis (that have been applied to other porous materials) [28], are promising for alternative COF preparation routes with enhanced properties as well.

## 4. Conclusion

In summary, COFs prepared via a static method display an outstretched, open polymer network, with a relatively lower contribution of intermolecular NDI-based interactions. On the other hand, a high intensity of stirring during synthesis yields a COF polymer network that is more aggregated in micro- and nano-length scales, which causes an overall higher contribution of intermolecular NDI-based interactions. We anticipate that utilisation of these synthesis strategies for NDI-COFs will affect their electrochemical device performance, because of its reliance on charge transport between aggregated NDI-based polymer chains [29]. While the effects have been shown for one COF system only, we expect that the route is more generic and can be applied successfully to other COF and COF related systems.

## CRediT authorship contribution statement

**Hugo Veldhuizen:** Writing – original draft, Visualization, Validation, Methodology, Investigation, Formal analysis, Data curation,

Conceptualization. **Sybrand van der Zwaag:** Writing – review & editing, Validation, Supervision, Methodology, Formal analysis, Conceptualization. **Monique van der Veen:** Writing – review & editing, Validation, Supervision, Formal analysis, Conceptualization.

## Declaration of competing interest

The authors declare that they have no known competing financial interests or personal relationships that could have appeared to influence the work reported in this paper.

## Data availability

The data concerning the characterization of the materials described in this work can be accessed and used by others for further studies at 4TU.ResearchData : https://doi.org/10.4121/20343237

## Acknowledgments

The authors thank Dr. Lorenzo Botto and Dr. Hugo Perrin for valuable discussions regarding reactor design, experimental parameters, and shear rate estimations. The authors also thank Ing. Bahiya Ibrahim for her assistance during the photoluminescence measurements.

## Appendix A. Supplementary data

Supplementary data to this article can be found online at https://doi.org/10.1016/j.micromeso.2022.112122.

## References

[1] T. Ma, E.A. Kapustin, S.X. Yin, L. Liang, Z. Zhou, J. Niu, L.-H. Li, Y. Wang, J. Su, J. Li, X. Wang, W.D. Wang, W. Wang, J. Sun, O.M. Yaghi, Science 361 (2018) 48–52, https://doi.org/10.1126/science.aat7679.

[2] K. Zhang, K.O. Kirlikovali, R.S. Varma, Z. Jin, H.W. Jang, O.K. Farha, M. Shokouhimehr, ACS Appl. Mater. Interfaces 12 (2020) 27821–27852, https://doi.org/10.1021/acsami.0c06267.

[3] M. Calik, F. Auras, L.M. Salonen, K. Bader, I. Grill, M. Handloser, D.D. Medina, M. Dogru, F. Löbermann, D. Trauner, A. Hartschuh, T. Bein, J. Am. Chem. Soc. 136 (2014) 17802–17807, https://doi.org/10.1021/ja509551m.

[4] H. Furukawa, O.M. Yaghi, J. Am. Chem. Soc. 131 (2009) 8875–8883, https://doi.org/10.1021/ja9015765.

[5] W. Wang, M. Zhou, D. Yuan, J. Mater. Chem. 5 (2017) 1334–1347, https://doi.org/10.1039/C6TA09234A.

[6] R. van der Jagt, A. Vasileiadis, H. Veldhuizen, P. Shao, X. Feng, S. Ganapathy, N. C. Habisreutinger, M.A. van der Veen, C. Wang, M. Wagemaker, S. van der Zwaag, A. Nagai, Chem. Mater. 33 (2021) 818–833, https://doi.org/10.1021/acs.chemmater.0c03218.

[7] N. Fernando, H. Veldhuizen, A. Nagai, S. Van der Zwaag, A. Abdelkader, Materials 15 (2022) 4, https://doi.org/10.3390/ma15010004.

[8] S. Patwardhan, A.A. Kocherzhenko, F.C. Grozema, L.D.A. Siebbeles, J. Phys. Chem. C 115 (2011) 11768–11772, https://doi.org/10.1021/jp202399u.

[9] Y. Wu, S. Schneider, C. Walter, A.H. Chowdhury, B. Bahrami, H.C. Wu, Q. Qiao, M. F. Toney, Z. Bao, J. Am. Chem. Soc. 142 (2020) 392–406, https://doi.org/10.1021/jacs.9b10935.

[10] D. Fazzi, M. Caironi, Phys. Chem. Chem. Phys. 17 (2015) 8573–8590, https://doi.org/10.1039/C5CP00523J.

[11] M. Schrimpf, J. Esteban, H. Warmeling, T. Färber, A. Behr, A.J. Vorholt, AIChE J. 67 (2021) 1–24, https://doi.org/10.1002/aic.17228.

[12] Q. Fang, Z. Zhuang, S. Gu, R.B. Kaspar, J. Zheng, J. Wang, S. Qiu, Y. Yan, Nat. Commun. 5 (2014) 4503, https://doi.org/10.1038/ncomms5503.

[13] A.V. Neimark, Y. Lin, P.I. Ravikovitch, M. Thommes, Carbon 47 (2009) 1617–1628, https://doi.org/10.1016/j.carbon.2009.01.050.

[14] C. Kessler, R. Schuldt, S. Emmerling, B.V. Lotsch, J. Kästner, J. Gross, N. Hansen, Microporous Mesoporous Mater. 336 (2022), 11796, https://doi.org/10.1016/j.micromeso.2022.111796.

[15] S.H. Kang, S.G. Lee, W.M. Jung, M.C. Kim, W.S. Kim, C.K. Choi, R.S. Feigelson, J. Cryst. Growth 254 (2003) 196–205, https://doi.org/10.1016/S0022-0248(03)01152-7.

[16] G. González, E. Colmenar, G. Diaconu, F. Alarcia, M. Manea, M. Paulis, M. J. Barandiaran, J.R. Leiza, J.C. de la Cal, J.M. Asua, Macromol. React. Eng. 3 (2009) 233–240, https://doi.org/10.1002/mren.200900015.

[17] L. Guérin, C. Coufort-Saudejaud, A. Liné, C. Frances, J. Colloid Interface Sci. 491 (2017) 167–178, https://doi.org/10.1016/j.jcis.2016.12.042.

[18] F.J. Trindade, G.J.T. Fernandes, A.S. Araújo, V.J. Fernandes Jr., B.P.G. Silva, R. Y. Nagayasu, M.J. Politi, F.L. Castro, S. Brochsztain, Microporous Mesoporous Mater. 113 (2008) 463–471, https://doi.org/10.1016/j.micromeso.2007.12.013.

[19] L. Zhang, Y. Zhou, M. Jia, Y. He, W. Hu, Q. Liu, J. Li, X. Xu, C. Wang, A. Carlsson, S. Lazar, A. Meingast, Y. Ma, J. Xu, W. Wen, Z. Liu, J. Cheng, H. Deng, Matter 2 (2020) 1049–1063, https://doi.org/10.1016/j.matt.2020.01.019.

[20] S. Maniam, H.F. Higginbotham, T.D.M. Bell, S.J. Langford, Chem. Eur J. 25 (2019) 7044–7057, https://doi.org/10.1002/chem.201806008.

[21] M. Pandeeswar, H. Khare, S. Ramakumar, T. Govindaraju, RSC Adv. 4 (2014) 20154–20163, https://doi.org/10.1039/C3RA47257D.

[22] P. Li, J.M. Maier, J. Hwang, M.D. Smith, J.A. Krause, B.T. Mullis, S.M.S. Strickland, K.D. Shimizu, Chem. Commun. 51 (2015) 14809–14812, https://doi.org/10.1039/C5CC06140G.

[23] M.D. Gujrati, N.S.S. Kumar, A.S. Brown, B. Captain, J.N. Wilson, Langmuir 27 (2011) 6554–6558, https://doi.org/10.1021/la2012809.

[24] N.A. Kukhta, D. Volyniuk, J.V. Grazulevicius, G. Sini, J. Mater. Chem. C 6 (2018) 1679–1692, https://doi.org/10.1039/C7TC05798A.

[25a] R. Steyrleuthner, M. Schubert, I. Howard, B. Klaumünzer, K. Schilling, Z. Chen, P. Saalfrank, F. Laquai, A. Facchetti, D. Neher, J. Am. Chem. Soc. 134 (2012) 18303–18317, https://doi.org/10.1021/ja306844f.

[25b] X. Li, Q. Gao, J. Aneesh, H. Sen Xu, Z. Chen, W. Tang, C. Liu, X. Shi, K.V. Adarsh, Y. Lu, K.P. Loh, Chem. Mater. 30 (2018) 5743–5749, https://doi.org/10.1021/acs.chemmater.8b02560.

[26] Y. Zhao, X. Liu, Y. Li, M. Xia, T. Xia, H. Sun, Z. Sui, X. Hu, Q. Chen, Microporous Mesoporous Mater. 319 (2021), 111046, https://doi.org/10.1016/j.micromeso.2021.111046.

[27] L. Zhang, L. Yi, Z.-J. Sun, H. Deng, Aggregate 2 (2021), e24, https://doi.org/10.1002/agt2.24.

[28] B. Szczęśniak, S. Borysiuk, J. Choma, M. Jaroniec, Mater. Horiz. 7 (2020) 1457–1473, https://doi.org/10.1039/d0mh00081g.

[29] S. Wang, S. Fabiano, S. Himmelberger, S. Puzinas, X. Crispin, A. Salleo, M. Berggren, Proc. Natl. Acad. Sci. U. S. A 112 (2015) 10599–10604, https://doi.org/10.1073/pnas.1501381112.

[30] Data related to the paper is stored at the 4TU.Research Data repository. https://doi.org/10.4121/20343237.